2014-05

Uptake of different crystal structures of TiO2 nanoparticles by Caco-2 intestinal cells

Gitrowski, C

10.1016/j.toxlet.2014.02.014
Toxicology Letters
Elsevier BV

Toxicology Letters 226 (2014) 264–276

Contents lists available at ScienceDirect

Toxicology Letters

journal homepage: www.elsevier.com/locate/toxlet

Uptake of different crystal structures of TiO_2 nanoparticles by Caco-2 intestinal cells

Constantinos Gitrowski*, Aliaa R. Al-Jubory, Richard D. Handy

School of Biomedical & Biological Sciences, University of Plymouth, Drake Circus, Plymouth PL4 8AA, UK

HIGHLIGHTS

- We studied the uptake of differing nanoTiO_2 crystal structures in Caco-2 cells.
- Cells exhibited saturable uptake of TiO_2, which was influenced by crystal structure.
- Results suggest energy mediated vesicular processes are involved in uptake of TiO_2.
- TiO_2 exposure appears to disturb some aspects of electrolyte status in Caco-2 cells.
- TiO_2 crystal structure should be accounted for in dietary exposure hazard assessments.

ARTICLE INFO

Article history:
Received 9 August 2013
Received in revised form 12 February 2014
Accepted 17 February 2014
Available online 25 February 2014

Keywords:
Caco-2
Uptake mechanism
Endocytosis
Electrolyte homeostasis
Titanium dioxide nanoparticles

ABSTRACT

The gastrointestinal uptake of different crystal structures of TiO_2 was investigated using Caco-2 intestinal cells. Caco-2 monolayers exhibited time-dependent, saturable uptake of Ti from TiO_2 exposures of 1 mg l^{-1} over 24 h, which was influenced by crystal type. Initial uptake rates were 5.3, 3.73, 3.58 and 4.48 nmol mg^{-1} protein h^{-1} for bulk, P25, anatase and rutile forms respectively. All exposures caused elevations of Ti in the cells relative to the control (ANOVA $P < 0.05$). Electron micrographs of the Caco-2 monolayer showed the presence of particles inside the cells, and energy dispersive spectroscopy (EDS) confirmed the composition as TiO_2. Incubating the cells with 120 IU nystatin (putative endocytosis inhibitor) or 100 μmol l^{-1} vanadate (ATPase inhibitor) caused large increases in Ti accumulation for all crystal types relative to controls (ANOVA $P < 0.05$), except for the rutile form with vanadate. Incubating the cells with 90 μmol l^{-1} genistein (tyrosine kinase inhibitor) or 27 μmol l^{-1} chloropromazine (clathrin-mediated endocytosis inhibitor) caused a large decrease in Ti accumulation relative to the controls (ANOVA $P < 0.05$). Cell viability measures were generally good (low LDH leak, normal cell morphology), but there were some changes in the electrolyte composition (K^+, Na^+, Ca^{2+}, Mg^{2+}) of exposed cells relative to controls. A rise in total Ca^{2+} concentration in the cells was observed for all TiO_2 crystal type exposures. Overall, the data shows that Ti accumulation for TiO_2 NP exposure in Caco-2 cells is crystal structure-dependent, and that the mechanism(s) involves endocytosis of intact particles.

1. Introduction

There is growing interest in the use of engineered nanomaterials (ENMs) in the food sector with suggested applications including the encapsulation of essential nutrients, the inclusion of nano minerals in food, and the use of ENMs as antibacterial agents to improve the shelf life or packaging of perishable goods (Aitken et al., 2006; Chaudry et al., 2008; Tiede et al., 2008). ENMs are also used in oral personal care products (e.g., tooth pastes), proposed for medicines that are intended for ingestion (Garnett and Kallinteri, 2006), and in drinking water technology (Handy and Shaw, 2007). It is therefore clear that humans are likely to be exposed to ENMs by the oral route, but current understanding of the bioavailability and uptake mechanisms of ENMs across the gut epithelium is limited (Panessa-Warren et al., 2006; Bouwmeester et al., 2009).

Bulk forms of titanium dioxide (TiO_2) have been used for many years in foods as a whitening agent (E 171), and estimates of daily ingestion rates summed for all forms of TiO_2 are between 5 and 50 mg in Europe and the USA (Lomer et al., 2000; Weir et al., 2012). It is likely that a fraction of the traditional ingested bulk

* Corresponding author.
E-mail addresses: constantinos.gitrowski@plymouth.ac.uk (C. Gitrowski), aliaa.al-jubory@plymouth.ac.uk (A.R. Al-Jubory), R.Handy@plymouth.ac.uk (R.D. Handy).

http://dx.doi.org/10.1016/j.toxlet.2014.02.014

TiO_2 was incidentally at the nano scale (estimated at around 35% (Weir et al., 2012)), and with engineered TiO_2 nanoparticles (NPs) now being available, it seems likely that increased ingestion of nano forms of TiO_2 will occur (Weir et al., 2012). Studies with ultrafine (<100 nm) TiO_2 particles have shown respiratory toxicity and epithelial inflammation of the lung in rodents (e.g., Ferin and Oberdorster, 1985; Ferin et al., 1992; Bermudez et al., 2004; Warheit et al., 2007). Like the lung, the gut also consists of mucous epithelia and there are concerns that TiO_2 NPs may be toxic to the gastrointestinal tract.

In vivo exposures using gut gavage to administer salines containing TiO_2 NPs have confirmed oral toxicity in rodents. Wang et al. (2007) exposed mice to ultrafine (25 or 80 nm) or fine (155 nm) TiO_2 particles by single oral gavage. Although no clear acute mortality occurred, changes to serum biochemical parameters indicating some loss of liver function and liver pathology (inflammation, necrosis) was observed (Wang et al., 2007). *In vivo* studies with other metals have also shown toxicity to the internal organs with oral gavage (Cu NPs, Chen et al., 2006; Zn NPs, Wang et al., 2006). In the latter, the symptoms also included gastrointestinal tract irritation (vomiting and diarrhoea) for the first few days (5 g kg^{-1} body weight of nano scale Zn, 58 nm diameter NPs). However, the few studies where the TiO_2 has been incorporated into animal feed show little systemic toxicity (e.g., fish, Ramsden et al., 2009; rat, Jani et al., 1994) indicating that the bioavailability of Ti in food is low.

There is some evidence for the uptake of Ti and/or TiO_2 NPs across the gut. Al-Jubory and Handy (2012) recently reported nystatin-sensitive transepithelial uptake of Ti from TiO_2 NPs across the isolated perfused intestine of trout, and found resting Ti uptake rates of around 1–3.4 nmol g^{-1} h^{-1}; similar to that of other non-essential divalent metals (e.g., Handy, 2003). In humans, particle size and dose-dependent increase of blood total Ti concentration following oral ingestion of anatase TiO_2 have been observed (Bockmann et al., 2000), providing some evidence for a particle size-effect on dietary uptake. Studies using cultured Caco-2 cells (a human-derived intestinal cell line) also suggest some Ti uptake, possibly of intact particles, without disruption of the epithelium (Koeneman et al., 2010).

However, the exact mechanism of how TiO_2 NPs are taken up by the gut epithelium is unclear. The possibilities include uptake of dissolved metal ions by dissolution of the particles in the gut lumen or in the mucus layer on the epithelial surface; and/or direct uptake of NPs by endocytosis-related pathways at the mucosal membrane (see review by Shaw and Handy, 2011 on nano metals). It is also unclear if the bulk material uses the same uptake pathway as the equivalent nano form. The situation is further complicated by the existence of several different crystal structures of TiO_2 including brookite, anatase, and rutile forms (the latter two being more commonly produced; Chen and Mao, 2007). Although cell culture studies have suggested some differences in the toxicities of the rutile and anatase forms (mostly in lung epithelial cells, Sayes et al., 2006; Singh et al., 2007; Wang et al., 2008), it is not clear if crystal structure influences the rate of uptake of Ti from TiO_2 NPs by gut cells, or if the different forms have different uptake mechanisms.

The overall aims of this research was to demonstrate the utility of the nascent Caco-2 cell line for Ti metal accumulation studies with TiO_2 NPs and then to compare the uptake of Ti from the bulk and nano forms (size effect), as well as the effects of different crystal structures (anatase and rutile). The approach used electrically tight, confluent monolayers of Caco-2 cells at 4–5 days old to enable fundamental metal uptake studies without the confounding factor of incidental nutritional uptake by non-specific processes in the aged epithelium (e.g., absorptive food vacuoles). The experiments included detailed pharmacological investigations of solute transport pathways for metals, as well as pharmacological studies to establish whether the different sizes or forms of TiO_2 were using different pathways to enter the cells. Finally, measurements of electrolytes in the cells, biochemical measurements on cell integrity, and electron microscopy investigations were made in the experiments to understand the physiological basis of any differences observed.

2. Materials and methods

Several experiments were performed using confluent monolayers of Caco-2 cells in culture medium (see below). The first series determined the total Ti metal accumulation in Caco-2 cells exposed to 1 mg l^{-1} of different forms of TiO_2 (bulk, nano P25 which was a mix of 25% rutile and 75% anatase, nano anatase, or nano rutile) over 24 h. Measurements also included effects on cell viability (LDH release, cell morphology) and electrolyte concentrations. The second series of experiments involved pharmacological investigations to determine whether or not the observed Ti metal accumulation involved either solute transport or endocytosis-related pathways for uptake at the mucosal (apical) membrane. In the third series of experiments, after having pharmacologically identified both solute transport and likely endocytosis components to Ti accumulation, the details were explored with more specific inhibitors of the possible routes involved for the different forms of TiO_2. In the present study, the authors adopt the same precise terminology for metal accumulation as used by Al-Jubory and Handy (2012). All data on Ti accumulation were normalized as a total Ti metal concentration in the cells, expressed as nmol Ti metal mg^{-1} cell protein (not TiO_2 compound), and is distinguish from the mg l^{-1} of TiO_2 compound added to the cell culture media when confirming the exposure. The phrase "total Ti metal concentrations" is used to mean the total mass concentration of Ti (not TiO_2 compound) in the cells or relevant media determined by inductively coupled plasma optical emission spectroscopy (ICP-OES, Varian 725 ES, see below). It does not infer anything about whether the Ti is present as particulate TiO_2 or as a dissolved Ti species. The term "Ti accumulation" is used to mean a net increase in the total Ti metal concentration in the cells over time, determined by ICP-OES of the digested cells.

2.1. Cell culture

A human intestinal cell line, Caco-2 (brush border expressing, European collection of cell cultures; catalogue no: 86010202; the supplier indicated that these cells were of the same origin as the ATCC HTB-37 Caco-2 cell line) was routinely incubated in 75 cm^2, 200 ml flasks (Iwaki T75, Japan) containing 15 ml of Dulbecco's modified eagle medium (DMEM) supplemented with 10% fetal bovine serum (FBS), 1% glutamine and 1% penicillin-streptomycin (100 IU Penicillin-100 μg ml^{-1} Streptomycin), at 37 °C and gassed with 95% air: 5% CO_2. The DMEM, FBS, glutamine and penicillin-streptomycin was obtained from Lonza (Verviers, Belgium). For routine maintenance, the medium was changed every 48 h and the cells were sub-cultured by trypsinization. Experiments were conducted on cells between passage 60–75 (cells were purchased at passage 45) and antibiotics were withdrawn to avoid possible interference with ion transport at least 2 passages before seeding the cells into 6-well plates (Iwaki microplates, Japan) for experiments. Preliminary trials were conducted to determine the optimum seeding density and time to confluence of the cells in 6-well plates by measuring the electrical resistance of the epithelium using an xCelligence real time label free cellular analysis system (Real-Time Cell Analyzer (RTCA), Roche Applied Science). In brief, the instrument monitors the change in electrical impedance associated with the electrical coupling of the epithelium during cell growth. Cells were grown on gold-coated wells (electrode), as cells adhered and spread across the well surface, increases in impedance were recorded. When confluence is reached, the impedance value (cell index) remains constant. A seeding density of 5×10^4 cells cm^{-2} produced confluence by 24 h (See additional file 1). Subsequently for all experiments, cells were seeded at 5×10^4 cells cm^{-2} in the 6-well plates and after an initial 24 h of growth, the cells were left for a further 48 h to ensure both 100% confluence and that the cells were rested. The cells were also visually inspected (Phase contrast microscope, Olympus/CK30-F200, Japan) each day until they became confluent. Cell viability was checked by tryphan blue exclusion prior to seeding the flasks and 6-well plates. Flasks with less than 90% cell viability were discarded. Lactate dehydrogenase leak (LDH) was also checked (see below).

2.2. Stock dispersions and materials characterisation

Four different types of TiO_2 were used (manufacturer's information): (i) bulk TiO_2 powder (ACROS, Titanium (IV) oxide, New Jersey, USA), composed of 75% anatase and 25% rutile crystal forms (Al-Jubory and Handy, 2012), at a purity of 98.0–100.5% TiO_2. (ii) Ultrafine TiO_2 NP type "Aeroxide" P25 (DeGussa AG, supplied by Lawrence Industries, Tamworth, UK) with a crystal structure of 25% rutile and 75% anatase TiO_2 (purity was at least 99% TiO_2 maximum impurity stated was 1% Si), the average particle size was 21 nm. (iii) Anatase TiO_2 NP form (US Research Nanomaterials, Inc, Houston, Texas, USA) with purity of 99% and 10–25 nm average particle size. (iv) rutile TiO_2 NP form (US Research Nanomaterials, Inc, Houston, Texas, USA) with high purity, 99.9% and 30 nm average particle size. A

stock dispersion of 500 mg l^{-1} for each type of TiO_2 was made (no solvents) by dispersing the particles in 200 ml of ultrapure water (Millipore, deionised water) in a 500 ml pyrex glass container by vigorous manual shaking for 1–2 min. Preliminary studies identified the materials as source of bacterial infection to cell cultures and subsequently all stock dispersions and the dry powder were gamma irradiated to sterilise them (Red Perspex, Turntable Irradiation Geometry, Becton Dickinson, Plymouth, England). The radiation dose was 36.42 → 40.72 kGy for 10 h to ensure sterility before starting cell culture experiments, and optimised to ensure the radiation did not interfere with the crystal structure of the materials.

The particle characterisation followed a similar protocol to our previous studies with TiO_2 NPs in the intestine (Al-Jubory and Handy, 2012). Briefly, sub samples of the 500 mg l^{-1} stock dispersions made in ultrapure water were examined for primary particle size using transmission electron microscopy (TEM, JEOL-1200EX II) (Fig. 1). The primary particle size was 103.2 ± 16 nm (mean ± S.E.M., n = 7), 22.8 ± 0.6 nm (mean ± S.E.M., n = 169), 16.4 ± 2.4 nm (mean ± S.E.M., n = 6) and 30.8 ± 2.5 (mean ± S.E.M., n = 7) for bulk, P25, anatase and rutile, respectively.

The particle size distribution was also determined using nanoparticle tracking analysis (NTA, Nanosight LM10, Nanosight, Salisbury, UK, laser output set at 30 mW at 640 nm). In order to achieve reliable tracks of individual particles, a 10 mg l^{-1} dilution in ultrapure water of the concentrated 500 mg l^{-1} stocks were used. The dispersions gave a mean hydrodynamic diameter of 179.3 ± 13.7, 7.1 ± 4.1, 142.3 ± 14.4 and 88.3 ± 34.1 nm (mean ± S.E.M., n = 3), for bulk, P25, anatase and rutile, respectively (Fig. 1). Attempts were made to determine particle size distribution of the materials in DMEM culture media. However, the media alone contained a high background of apparent particulates (most likely NaCl crystals) and the DMEM media with supplements gave particle size distributions with a smallest bin size of around 30 nm and average hydrodynamic diameters for the whole sample around 156 nm. Furthermore, NTA of the DMEM with supplements gave very high particle number concentrations (90×10^6 particles) due to the presence of proteins, and would completely mask the particle counts due to TiO_2 (4–10 times lower than that of the culture media). Thus attempts to detect TiO_2 particle distributions in the culture media gave poor reproducibility by NTA due to this high background (See additional file 2).

2.3. Experiment 1: Time course of Ti accumulation from different forms of TiO_2

This experiment determined the time course of Ti accumulation for the different forms of TiO_2 in Caco-2 cells over 24 h. Confluent cells (72 h after seeding) were exposed to the cell culture media (as above minus antibiotics) containing 1 mg l^{-1} of either no added TiO_2 (control), bulk, P25, anatase or rutile forms of TiO_2. The six-well plate was the unit of replication in the experiment, with each plate contained cells with no TiO_2 additions (2 control wells), and a well for each of the test materials. At least three plates were prepared for each time point in the experiments (n = 3 replicates/time point). Dosing of the wells was performed by diluting the initial 500 mg l^{-1} stock to 10 mg l^{-1} TiO_2 in ultrapure water, and this secondary stock was mixed with fresh culture media (1 ml of the appropriate 10 mg l^{-1} TiO_2 stock: 9 ml DMEM) to obtain a final concentration of 1 mg l^{-1} TiO_2 for the exposures. Two ml of the appropriate media was pipetted into each well. Media and cells were then collected at 0, 2, 4, 6, 8 and 24 h of exposure for total Ti determination, electrolyte concentrations and LDH activity (see below).

2.4. Experiment 2: The effect of nystatin and vanadate incubation on Ti accumulation

Having established the time course of Ti accumulation in Caco-2 cells from exposure to the different forms of TiO_2 the next stage was to assess the effect of mucosal (apical) additions of nystatin (a putative endocytosis inhibitor, Lewis et al., 1977) and sodium orthovanadate (a P-type ATPase inhibitor which blocks active ion transport, Cantley et al., 1978) on Ti accumulation. Cells were grown and exposed to 1 mg l^{-1} of the forms of TiO_2 as above, except that 1 hour prior to dosing with the appropriate particles, cells were pre-incubated with either 120 IU ml^{-1} of nystatin (dose to produce 100% inhibition, Lewis et al., 1977), or 100 μmol l^{-1} sodium orthovanadate (enough to block metal transport in the intestine, Handy et al., 2000), compared to drug-free controls with and without added TiO_2 (n = 6 plates/treatment, with separate drug free controls). Inhibitors were dissolved in 500 ml of DMEM. This pre-incubation enabled the drugs to have direct contact with the cells without the risk of interference from the test materials (i.e., loss of bioavailable drug due to adsorption onto particles). The inhibitors remained in the media throughout the experiment, and the appropriate TiO_2 dose was simply added to the media after the initial 1 h pre-incubation. After 24 h cells and media were analysed as above.

2.5. Experiment 3: The effect of chloropromazine, genistein and amiloride on Ti accumulation

The second experiment above identified a nystatin-sensitive component to Ti accumulation, and this final series of experiments explored the details of what types of endocytosis-related mechanisms might be involved. Three different drugs were tested, and drug concentrations were selected after some range finding experiments. The drugs were: 27 μmol l^{-1} chloropromazine (a specific inhibitor of clathrin mediated endocytosis, Wang et al., 1993), 90 μmol l^{-1} genistein (a tyrosine kinase inhibitor, which prevents caveolae scission and disrupts the actin cytoskeleton, Nabi and Lee, 2003) and 1.25 mmol l^{-1} amiloride hydrochloride hydrate. The latter is a well-known blocker of epithelial Na^+ channels (Handy, 2003), but may also prevent non-specific macropinocytosis (Dameron and Harrison, 1998; Iverson et al., 2011). Amiloride and chloropromazine were dissolved in warm deionised water (to ensure all solids were in solution) at concentrations of 50 mmol l^{-1} and 3.7 mmol l^{-1} respectively. Genistein was dissolved in neat DMSO at a concentration of 9.25 mmol l^{-1}. The stock solutions of each drug were filter sterilised (0.22 μm, Millipore) to prevent bacterial infection of the cell cultures, prior to being diluted to the appropriate working concentrations (above) in the culture media. The experiments were conducted exactly as above (n = 6 plates/treatment, with separate drug free controls), except that cells were pre-incubated for 1 h with the appropriate drug prior to the 24 h TiO_2 exposure. Samples for Ti, electrolytes and LDH were collected at the end of the experiment.

2.6. Titanium and electrolyte determination in cells

Following careful removal of the culture media, the cells attached to the dish were washed twice with 2 ml of an isosmotic sucrose buffer (300 mmol l^{-1} sucrose, 0.1 mmol l^{-1} ethylenediaminetetraacetic acid (EDTA), 20 mmol l^{-1} 4-(2-hydroxyethyl)-1-piperazineethanesulfonic acid (HEPES), buffered to pH 7.4 with a few drops of 2 mol l^{-1} Trizma base) to remove any residual culture media and the external electrolytes therein. Cells were then carefully scraped off the bottom of the well (Fisher scientific cell scraper, 250 mm handle, 18 mm blade) and re-suspended in the well with 1 ml of a sucrose lysis buffer (the recipe above, but hypo-osmotic with only 30 mmol l^{-1} sucrose). The resulting homogenate was pipetted into 13 ml test tubes (Fischer Scientific) and sonicated (power 100 Watt, setting 8/speed 22.5 kHz, Misonix incorporated, XL2000-010, New York) for 30 s to ensure the lysed sample was well mixed. Each sample was then gently centrifuged for 1 min to remove debris (~160 g, Heraeus instruments, Biofuge *pico*, Germany) and a 200 μl aliquot of the supernatant taken fresh for LDH activity and protein determination (see below). The remaining 800 μl of the cell homogenate was digested in 1 ml of concentrated nitric acid (70%) at 70 °C for 4 h, and total Ti, Na^+, K^+, Ca^{2+} and Mg^{2+} determined by ICP-OES. Samples were vortexed for 20 s immediately prior to being drawn into the instrument to ensure mixing, and calibrations were performed with matrix-matched multi-elemental standards containing Ti, Na^+, K^+, Ca^{2+} and Mg^{2+} in 38% nitric acid. In the absence of certified reference tissues for TiO_2 particle analysis, spike recovery tests were performed. Samples of cell homogenates were spiked with 200 μl of 10 mg l^{-1} of the different forms of TiO_2 and showed procedural recoveries of 80.4 ± 4.2, 82.2 ± 1.5, 76.3 ± 4.7 and 75.7 ± 1.8% for bulk TiO_2, P25, anatse and rutile forms, respectively (mean ± S.E.M, n = 6 for each material type). Checks on analytical precision showed low coefficients of variation within and between samples (<5%).

Electrolyte concentrations in the cell homogenates were normalised to cell protein content. The latter was measured in triplicate using the bicinchoninic acid (BCA) method (MC155208, Pierce, Rockford, USA). Briefly, 15 μl of sample was added to 300 μl of the BCA reagents and the absorbance read at 570 nm in 96-well plates (VERSA max, Molecular Devices, Berkshire, UK) against bovine serum albumin standards. Calibrations spiked with and without 1 mg l^{-1} TiO_2 showed no interference with the assay or colour reagent (See additional file 3).

2.7. Lactate dehydrogenase activity

Lactate dehydrogenase activity was measured in the cell culture media overlying the cells (media LDH) and in the cell homogenates (cell LDH). For the former, 200 μl of cell culture media from each well was gently centrifuged for 1 min to remove any cell debris/turbidity (~160 × *g*, Heraeus instruments, Biofuge *pico*, Germany) and 100 μl of the resulting supernatant was used in the LDH assay. For the latter, 200 μl of cell homogenate was sonicated and centrifuged (as above) and then 100 μl of the cell supernatant was used in the LDH assay (Plummer, 1971). Briefly, 100 μl of sample (media or cell supernatant) were added to a reaction mixture (2800 μl of 0.6 mmol l^{-1} pyruvate in 50 mmol l^{-1} phosphate buffers at pH 7.4, plus 100 μl of 0.6 mmol l^{-1} NADH solution), mixed directly in a 3 ml cuvette and the change in absorbance measured over 2 minutes at 340 nm (Helios ß spectrophotometer). The specific activity of the LDH was then calculated using an extinction coefficient of 6.22×10^{-3} l mol^{-1} cm^{-1} for a path length of 1 cm. LDH activity is expressed as IU ml^{-1} (μmol min^{-1} ml^{-1}) of media. The percentage of LDH leak from the cells within each well was also estimated from the absolute total LDH content of each well (cells + media) divided by the LDH content of the media alone.

2.8. Cell morphology and scanning electron microscopy

Cell morphology was examined directly by phase contrast microscopy (Olympus/CK30-F200, Japan) during experiments, whilst separate runs of plates were carried out for detailed morphological investigations on fixed samples using bright field light microscopy and electron microscopy. Briefly for bright field light microscopy, cells were washed *in situ* on the cell culture dish with Dulbecco's phosphate buffered saline (DPBS, Lonza, Verviers, Belgium), then fixed with 5 ml of fresh methanol for 5 min, prior to staining with Giemsa (Giemsa's stain solution, IVD,

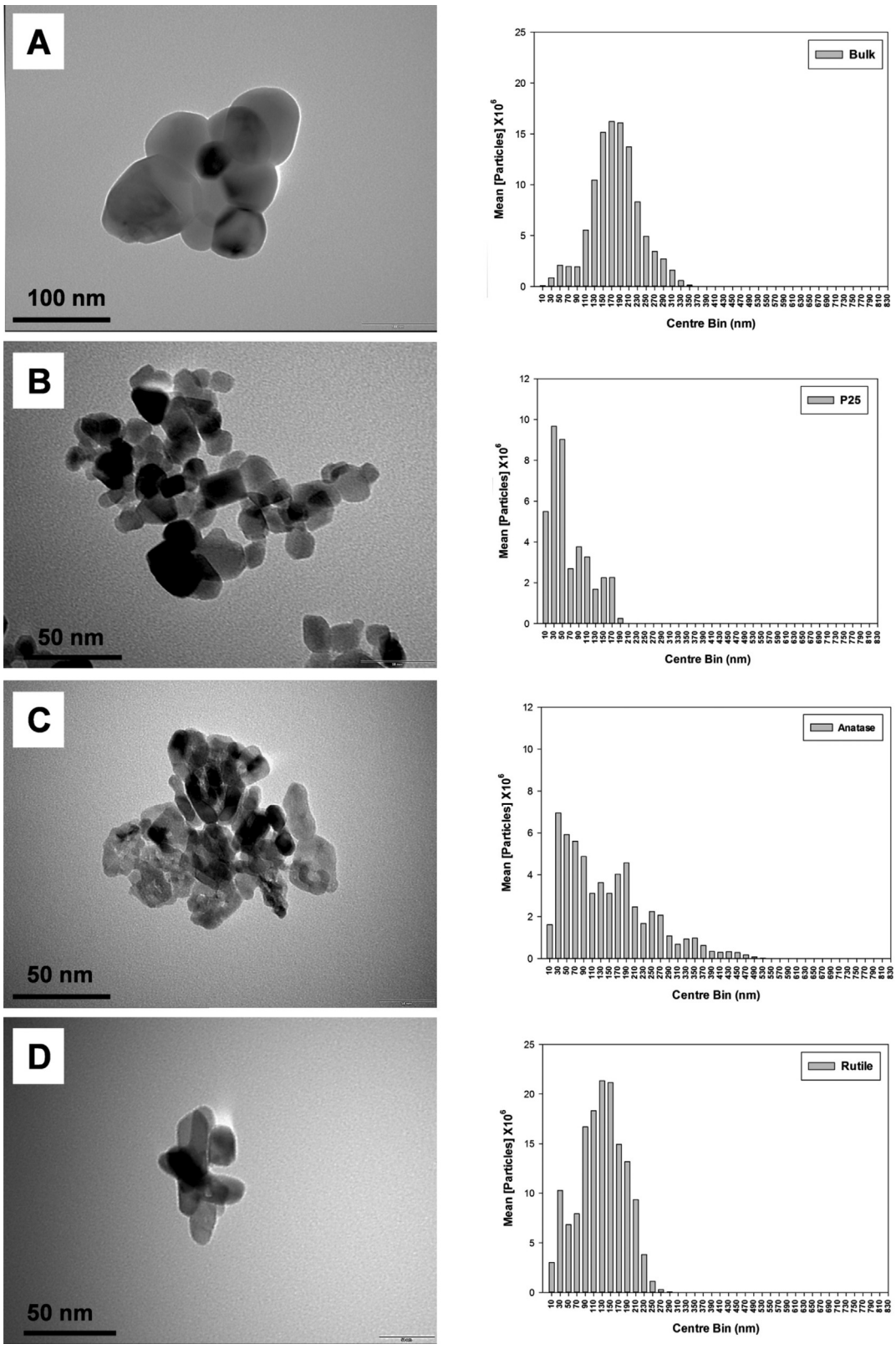

Fig. 1. Transmission Electron microscope (TEM) images showing primary particles, and particle size distributions by nanoparticle tracking analysis (hydrodynamic diameter, Nanosight LM10) of; (A) bulk TiO_2 particles, scale bar = 100 nm, (B) P25, scale bar = 50 nm, (C) anatase, scale bar = 50 nm and (D) rutile, scale bar = 50 nm at a concentration of 10 mg l^{-1} (dilutions of the 500 mg l^{-1} stocks) in Milliq water. Particle size distribution plots are individual examples from triplicate measurements.

England). Plates were examined wet using light microscopy (Nikon, 803923-Japan) and photographs taken using a digital camera (Pentax, K-X).

For scanning electron microscopy (SEM), the cells were fixed *in situ* on the culture plates and a disk cut out of the plate wells for mounting on SEM grids. Briefly, cells were washed in sucrose wash buffer (above) and fixed for 1 h in 2 ml of 2.5% glutaldehyde in cacodylate buffer (0.1 M sodium cacodylate in water followed by the drop wise addition of 0.2 M HCl to a pH of 7.4). The cells were then washed twice in cacodylate buffer prior to being dehydrated in a graded series of ethanol. Cells were

critically point dried and carbon coated (EMITECH-K850, K450X). Samples were imaged and elementally analysed (SEM, JEOL/JSM-7001F, Oxford Instruments INCA X-ray analysis system) using a 15 KV accelerating voltage, at a working distance of 10 mm.

A separate series of culture plates were prepared for transmission electron microscope (TEM) investigations (3 plates/treatment). It was not possible to obtain TEMs from cells cut directly from the bottom of the plastic cell culture plates. Instead, cells were grown on well inserts (Millipore Millicell hanging cell culture insert, 0.4 μm pore size designed for 12 well plates) for up to 21 days. Then, in order to increase the chances of observing particles in the individual cells by TEM, the microplates were exposed to 10 mg l^{-1} of each form of TiO_2 for 24 h (rather than the 1 mg l^{-1} used above). Inserts were fixed in 2.5% glutaraldehyde buffered in 0.1 M sodium cacodylate at pH 7.2 and post-fixed in 2% OsO_4. The specimens were then dehydrated in a graded series of ethanol, infiltrated with Spur's resin (Agar Scientific, Essex UK), and embedded into coffin moulds using pure resin. Thin sections were cut (>90 nm) and stained with 2% uranyl-acetate and lead citrate, then examined by transmission electron microscope (TEM, JEOL-1200EX II). For block face analysis of the samples, specimens were viewed in backscatter imaging mode at an accelerating voltage of 10 KV and elementally analysed (SEM, JEOL/JSM-7001F, Oxford Instruments INCA X-ray analysis system).

2.9. Statistics

Data were analysed using >StatGraphics Plus Version 5.1 and shown as means ± standard errors (S.E.M) unless otherwise stated. After checking data for kurtosis, skewedness, and unequal variance (Bartlett's test), one-way ANOVA followed by the least squares difference multiple range test was applied to analyse treatment effects, or time effects where appropriate. In the time course experiment, two-way ANOVA was used to determine treatment x time effects. Where data were non-parametric, the Kruskal–Wallis test (analysis by ranks) was used and differences were located using notched box and whisker plots. The Student's *t*-test was sometimes used to investigate the differences between pairs of data, or the Mann–Whitney *U* test where appropriate for non-parametric data. All statistical analysis used the default 95% confidence limit. Curve fitting for time-effects was performed using Sigma Plot Version 12.0. Curves were fitted to the raw data, although the figures show the mean values for convenience.

3. Results

3.1. Cell health and viability

The control cells (not exposed to TiO_2 or treated with drugs) showed normal morphology (day 4) during the experiments with the cells remaining confluent and attached to the dishes with intact apical membranes, orientated in the correct way with the presence of uniform microvilli. This was also supported by LDH activity which remained at around 0.2 IU ml^{-1} or less of cumulative LDH release over the 24 h duration of the experiments. The control cells also showed normal electrolyte levels with negligible variation in cell electrolyte concentrations. For example, in the time course experiment the electrolyte levels in control cells were (mean ± SEM, $n = 3$ plates/treatment): Na^+, 6359 ± 581; K^+, 867 ± 26; Ca^{2+}, 16 ± 4; and Mg^{2+}, 48 ± 1 nmol mg^{-1} protein. The controls across experiments and batches of cells, all had low membrane leak, and although electrolyte concentrations showed some variability when expressed per mg of cell protein, the values remained in the normal physiological range. For example, the control cells in the second experiment also showed cumulative LDH values in the media of 0.15 IU ml^{-1} or less, and the ranges of electrolyte concentrations in these controls (from $n = 6$ plates) were: Na^+, 4518 ± 533; K^+, 718 ± 14; Ca^{2+}, 11 ± 1; and Mg^{2+}, 43 ± 1 nmol mg^{-1} protein.

Similarly for the experiments with inhibitors, the control cells incubated with drugs but no TiO_2 showed normal morphology and remained adhered to the dishes. Cumulative LDH was low (mean ± SEM, $n = 6$ plates, between 0.15 ± 0.5 IU ml^{-1}) except for cells incubated with 1.25 mmol l^{-1} amiloride which exhibited a cumulative leak of 0.354 ± 0.026 IU ml^{-1} (Table 1). Metabolic and ion transporter inhibitors are expected to cause variations in electrolyte levels and some statistically significant changes occurred in the electrolyte concentrations relative to the appropriate no added drug controls without TiO_2 (Table 2). For example, additions of vanadate caused elevations of cell Ca^{2+} concentrations and depletion of K^+ consistent with ion diffusion down their respective electrochemical gradients. Additions of nystatin resulted in increases of all the major electrolytes in the cells compared to drug-free controls without TiO_2 present (Table 2). Conversely, additions of chloropromazine depleted cell K^+, Na^+ and Ca^{2+} (Table 2). Genistein notably caused a 2.7 fold increase in cell Ca^{2+} concentration, and also lowered cell Na^+. Amiloride caused the expected Na^+-depletion consistent with block of the epithelial Na^+ channel, but also caused K^+ and Ca^{2+} to rise compared to the drug free control without TiO_2 (Table 2).

Cells incubated with the different forms of TiO_2 also demonstrated low cumulative LDH leak (0.15 ± 0.05 IU ml^{-1}) and reasonably consistent electrolyte concentrations within the physiological range, although there were some TiO_2-dependent changes in ion concentrations (Table 2, see below).

3.2. Experiment 1: Time course of Ti accumulation from different forms of TiO_2

The time course of Ti accumulation for exposures to the different forms of TiO_2 is shown in Fig. 2. The unexposed control cells remained at a background metal concentration of around 2 nmol Ti mg^{-1} cell protein throughout. All the TiO_2 treatments showed a non-linear hyperbolic rise of the total Ti concentration in the cells, which achieved steady-state concentrations by 24 h. This saturable rise in net Ti accumulation by the cells occurred without similar elevations of cell Na^+ or K^+ concentrations which remained between 6500–9000 and 800–1000 nmol mg^{-1} protein respectively; indicating that the Ti response was Ti-specific and not an artefact of general electrolyte changes in the cells. There were some differences in the time courses of Ti accumulation for the different forms of TiO_2 (Fig. 2), and these were not explained by osmotic disturbances in the cells or by differences in membrane permeability across the treatments. For the latter, the cumulative

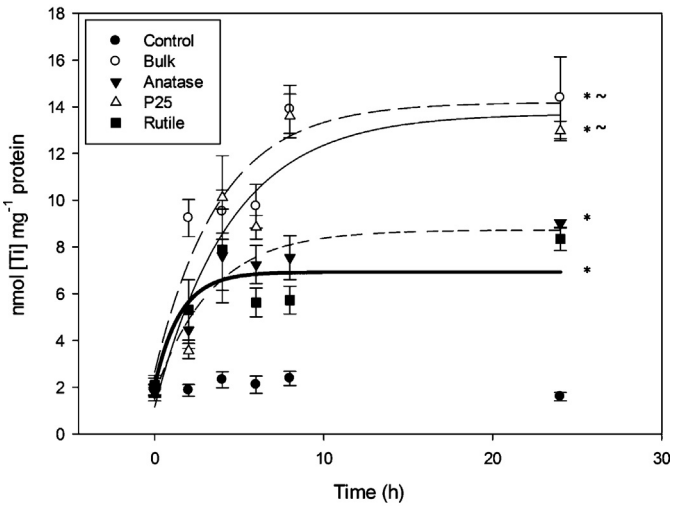

Fig. 2. (Experiment 1): Titanium accumulation in Caco-2 cells from exposures to 1 mg l^{-1} of different forms of TiO_2 for 24 h. Data points are means ± SEM ($n = 3$ replicates/treatment). Curves were fitted using Sigma plot version 12.0 to the raw data ($n = 3$ observations/treatment) using the rectangular hyperbola function ($f = y_0 + a \times (1 - \exp(-b \times x))$). Equations for the curve fits were as follows: For bulk $f = 2.64 + 11.54 \times (1 - \exp(-0.261 \times x))$, $r^2 = 0.901$; For P25, $f = 1.16 + 12.54 \times (1 - \exp(-0.22 \times x))$, $r^2 = 0.875$; For anatase $f = 1.71 + 7.01 \times (1 - \exp(-0.3017 \times x))$, $r^2 = 0.952$; For rutile $f = 2.07 + 4.86 \times (1 - \exp(-0.67 \times x))$, $r^2 = 0.731$. The unexposed control showed no time-dependent changes and therefore a curve was not fitted. Accumulation of all titanium forms is significantly different to the controls (ANOVA $P < 0.05$ (*)) at 24 h. Accumulation of Bulk and P25 titanium forms at 24 h is significantly greater than the anatase and rutile forms (ANOVA $P < 0.05$ (~)).

Table 1
Cumulative LDH leak in Caco-2 cells at 24 h following exposure to 1 mg l^{-1} of different TiO_2 forms in the presence or absence of inhibitors.

Treatment		No drug	Chloropromazine (27 μmol l^{-1})	Genistein (90 μmol l^{-1})	Amiloride HCL (1.25 mmol l^{-1})
Control	IU ml^{-1} Extracellular	0.129 ± 0.009^{a}	0.158 ± 0.015^{a}	0.184 ± 0.019^{a}	0.354 ± 0.026^{b}
	IU ml^{-1} Intracellular	1.565 ± 0.034^{a}	1.558 ± 0.033^{a}	1.584 ± 0.023^{a}	1.277 ± 0.051^{b}
	% LDH leak	7.723 ± 0.522^{a}	9.346 ± 0.918^{a}	10.56 ± 1.08^{a}	21.99 ± 1.54^{b}
Bulk	IU ml^{-1} Extracellular	0.153 ± 0.014^{a}	0.143 ± 0.023^{a}	0.176 ± 0.014^{a}	0.407 ± 0.040^{b}
	IU ml^{-1} Intracellular	1.577 ± 0.039^{a}	1.620 ± 0.017^{a}	1.622 ± 0.036^{a}	1.420 ± 0.054^{a}
	% LDH leak	8.950 ± 0.717^{a}	8.216 ± 1.270^{a}	9.872 ± 0.56^{a}	22.48 ± 1.39^{b}
P25	IU ml^{-1} Extracellular	0.199 ± 0.014^{a}	0.177 ± 0.024^{a}	0.212 ± 0.027^{a}	0.404 ± 0.031^{b}
	IU ml^{-1} Intracellular	1.635 ± 0.094^{a}	1.658 ± 0.109^{a}	1.593 ± 0.011^{a}	1.263 ± 0.109^{b}
	% LDH leak	10.95 ± 0.136^{a}	9.668 ± 0.686^{a}	11.88 ± 1.39^{a}	24.81 ± 3.15^{b}
Anantase	IU ml^{-1} Extracellular	0.159 ± 0.017^{a}	0.164 ± 0.012^{a}	0.196 ± 0.054^{a}	0.288 ± 0.054^{b}
	IU ml^{-1} Intracellular	1.578 ± 0.031^{a}	1.551 ± 0.022^{a}	1.609 ± 0.018^{a}	1.072 ± 0.052^{b}
	% LDH leak	9.271 ± 0.947^{a}	9.691 ± 0.766^{a}	10.88 ± 2.703^{a}	21.13 ± 2.92^{b}
Rutile	IU ml^{-1} Extracellular	0.152 ± 0.011^{a}	0.138 ± 0.007^{a}	0.185 ± 0.030^{a}	0.413 ± 0.064^{b}
	IU ml^{-1} Intracellular	1.550 ± 0.013^{a}	1.539 ± 0.044^{a}	1.604 ± 0.047^{a}	1.404 ± 0.054^{b}
	% LDH leak	9.086 ± 0.623^{a}	8.374 ± 0.578^{a}	10.46 ± 1.63^{a}	22.81 ± 2.11^{b}

Data are expressed as means ± S.E.M. ($n = 6$). Values are expressed as μmol min^{-1} ml^{-1} at 37 °C (IU ml^{-1}). Different letters indicate statistically significant differences within rows (ANOVA $P > 0.05$).

LDH leak by 24 h remained low, at 0.15 ± 0.5 IU ml^{-1} (not statistically different from the control, and no material-type effect was observed, ANOVA, $P < 0.05$, Table 1). The net Ti accumulation by 24 h was in the following order by material-type: bulk and P25 nano > anatase > rutile > unexposed controls. The bulk material and P25 nano TiO_2 showed the largest net Ti accumulation in 24 h, saturating at 14.1 and 13.64 nmol mg^{-1} protein respectively, but were not statistically different from each other by 24 h (ANOVA $P < 0.05$). The anatase form showed approximately 40% less Ti accumulation than either the P25 or bulk material (statistically different by 24 h, Fig. 2). There were also some differences in Ti accumulation from the pure anatase and rutile forms, with the latter showing saturation at a slightly lower Ti concentration (Fig. 2). However, the mean values at 24 h were not statistically different (ANOVA, $P < 0.05$). The initial Ti accumulation rates calculated from the curves (Fig. 2) followed a similar pattern with Ti accumulation from the bulk and rutile being faster than those from anatase or P25. The initial accumulation rates were 5.3, 3.73, 3.58 and 4.48 nmol mg^{-1} protein h^{-1}

Table 2
(Series 2 and 3): The total intracellular K^+, Na^+ Ca^{2+}, and Mg^{2+} nmol [Metal] mg^{-1} protein following exposure to 1 mg l^{-1} TiO_2 forms in the presence and absence of drugs (Series 2: nystatin and vanadate; Series 3, chloropromazine, genistein, amiloride HCL) for 24 h.

Electrolytes (nmol mg^{-1} protein)						
		Control	Bulk	P25	Anatase	Rutile
Experiment 2						
K^+	No Drug	718.8 ± 14.2^{a}	663.9 ± 28.3^{b}	643.8 ± 19.6^{b}	637.9 ± 27.6^{b}	611.1 ± 11.4^{b}
	Nystatin	$927.9 \pm 50.8^{\#a}$	$828.8 \pm 62.3^{\#b}$	$815.7 \pm 30.0^{\#b}$	$822.7 \pm 57.9^{\#b}$	$807.1 \pm 41.2^{\#b}$
	Vanadate	$466.8 \pm 43.8^{\#a}$	$479.6 \pm 36.9^{\#a}$	$469.3 \pm 26.9^{\#a}$	$513.3 \pm 16.9^{\#a}$	$490.7 \pm 37.1^{\#a}$
Na^+	No Drug	4518 ± 160^{a}	4666 ± 576^{a}	4793 ± 231^{a}	5109 ± 624^{a}	4319 ± 350^{a}
	Nystatin	$6303 \pm 468^{\#a}$	5253 ± 445^{a}	5144 ± 308^{a}	5748 ± 455^{a}	5202 ± 417^{a}
	Vanadate	$3632 \pm 427^{\#a}$	4246 ± 406^{a}	$3982 \pm 311^{\#a}$	$4457 \pm 216^{\#a}$	4534 ± 568^{a}
Ca^{2+}	No Drug	10.6 ± 1.2^{a}	14.3 ± 7.0^{a}	28.0 ± 12.4^{b}	20.8 ± 5.4^{b}	19.1 ± 8.2^{a}
	Nystatin	$25.7 \pm 9.4^{\#a}$	19.8 ± 2.2^{b}	27.8 ± 5.7^{a}	14.4 ± 4.6^{b}	17.7 ± 3.1^{b}
	Vanadate	$20.9 \pm 3.6^{\#a}$	$25.2 \pm 4.6^{\#a}$	18.0 ± 7.2^{a}	18.7 ± 4.1^{a}	$29.1 \pm 2.4^{\#b}$
Mg^{2+}	No drug	42.6 ± 1.1^{a}	47.8 ± 2.2^{b}	53.4 ± 2.7^{b}	49.8 ± 1.4^{b}	50.7 ± 1.5^{b}
	Nystatin	$56.2 \pm 2.9^{\#a}$	$55.3 \pm 2.8^{\#a}$	55.0 ± 1.8^{a}	$56.2 \pm 4.4^{\#a}$	55.0 ± 3.1^{a}
	Vanadate	$30.9 \pm 3.4^{\#a}$	$38.9 \pm 3.1^{\#b}$	$39.4 \pm 2.7^{\#b}$	43.8 ± 2.3^{b}	$40.9 \pm 2.8^{\#b}$
Experiment 3						
K^+	No Drug	684.2 ± 16.8^{a}	650.2 ± 31.8^{b}	655.4 ± 19.7^{b}	638.5 ± 25.0^{b}	600.8 ± 34.4^{b}
	Chloropromazine	$565.2 \pm 16.2^{\#a}$	$553.3 \pm 40.3^{\#a}$	$534.4 \pm 22.2^{\#a}$	$561.3 \pm 33.2^{\#a}$	$550.9 \pm 18.5^{\#a}$
	Genistein	642.5 ± 31.3^{a}	634.6 ± 35.8^{a}	686.5 ± 36.5^{a}	653.7 ± 33.6^{a}	663.4 ± 19.3^{a}
	Amiloride	$1039.8 \pm 273^{\#a}$	$977.1 \pm 154^{\#a}$	$771.7 \pm 120^{\#b}$	$795.0 \pm 199^{\#b}$	$827.1 \pm 121^{\#a}$
Na^+	No Drug	6007 ± 359^{a}	5671 ± 474^{a}	5654 ± 365^{a}	5528 ± 477^{a}	4251 ± 337^{a}
	Chloropromazine	$1364 \pm 160^{\#a}$	$1266 \pm 136^{\#a}$	$1100 \pm 73^{\#a}$	$1070 \pm 50^{\#a}$	$1041 \pm 45^{\#a}$
	Genistein	$3858 \pm 396^{\#a}$	$4038 \pm 257^{\#a}$	$4080 \pm 342^{\#a}$	$4176 \pm 208^{\#a}$	$4874 \pm 843^{\#a}$
	Amiloride	$4118 \pm 457^{\#a}$	$3708 \pm 902^{\#a}$	$3318 \pm 802^{\#a}$	$3358 \pm 1175^{\#a}$	$3067 \pm 521^{\#a}$
Ca^{2+}	No Drug	15.5 ± 1.6^{a}	28.5 ± 5.1^{b}	32.1 ± 7.3^{b}	26.9 ± 4.9^{b}	17.9 ± 1.4^{c}
	Chloropromazine	$12.5 \pm 1.3^{\#a}$	$12.8 \pm 1.6^{\#a}$	$11.7 \pm 1.5^{\#a}$	$12.2 \pm 0.8^{\#a}$	$10.1 \pm 1.2^{\#a}$
	Genistein	$48.3 \pm 8.1^{\#a}$	$37.0 \pm 2.9^{\#a}$	$38.2 \pm 7.7^{\#a}$	$40.5 \pm 2.4^{\#a}$	$36.1 \pm 7.1^{\#a}$
	Amiloride	$104.1 \pm 17.1^{\#a}$	$173.9 \pm 69.8^{\#a}$	$86.4 \pm 41.1^{\#a}$	$70.1 \pm 16.2^{\#a}$	$68.6 \pm 11.1^{\#a}$
Mg^{2+}	No Drug	40.2 ± 1.1^{a}	40.7 ± 0.6^{a}	41.5 ± 2.0^{a}	39.5 ± 0.9^{a}	37.7 ± 2.1^{b}
	Chloropromazine	$37.3 \pm 1.0^{\#a}$	38.8 ± 2.9^{a}	$36.2 \pm 1.7^{\#a}$	38.6 ± 2.4^{a}	38.3 ± 1.3^{a}
	Genistein	38.4 ± 1.6^{a}	40.6 ± 1.7^{b}	43.7 ± 2.7^{b}	42.4 ± 0.8^{b}	$43.9 \pm 0.2^{\#b}$
	Amiloride	$84.0 \pm 5.0^{\#a}$	$70.4 \pm 7.5^{\#a}$	$68.4 \pm 3.7^{\#a}$	$71.4 \pm 12.2^{\#a}$	$79.9 \pm 8.3^{\#a}$

Values are means ± S.E.M ($n = 6$ for each group) and are expressed as nmol mg^{-1} cell protein. Different letters indicate statistically significant differences within rows. (ANOVA $P < 0.05$). #Statistically significant difference of drug controls relative to 'no drug' controls within 'control' column (ANOVA $P < 0.05$). Series 2 is the data associated with experiment 2, series 3 is the data associated with experiment 3.

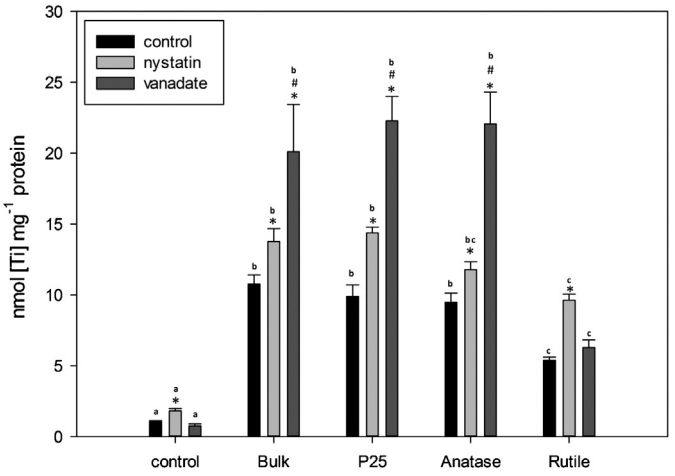

Fig. 3. (Experiment 2): Effect of nystatin and vanadate on Ti accumulation in Caco-2 cells incubated with 1 mg l^{-1} titanium forms at 24 h. The plots are means ± SEM ($n = 6$) from the replicate data and are expressed as 'nmol [Ti] mg^{-1} protein'. Statistical analysis at 24 h time point showed that the levels of accumulation relative to the no drug controls were different (ANOVA $P < 0.05$ (*)). Symbol (#) indicates statistical differences between vanadate and nystatin (ANOVA $P < 0.05$). Letters represent differences between materials within drug treatment (material- type effect) (ANOVA $P < 0.05$).

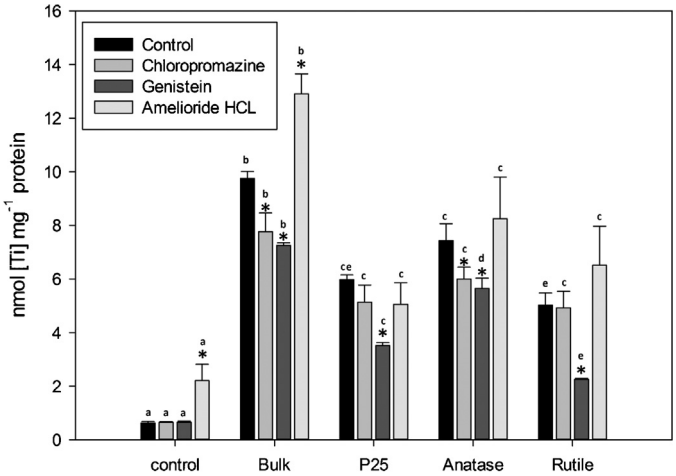

Fig. 4. (Experiment 3): Effects of chloropromazine, genistein and amiloride on Ti accumulation in Caco-2 cells incubated with 1 mg l^{-1} titanium forms at 24 h. The plots are means ± SEM ($n = 6$) from the replicate data and are expressed as 'nmol [Ti] mg^{-1} cell protein'. Statistical analysis at 24 h showed that the levels of accumulation relative to the no drug controls were different (ANOVA $P < 0.05$ (*)). Letters represent differences between materials within drug treatment (material- type effect) (ANOVA $P < 0.05$).

for bulk, P25, anatase and rutile respectively. The times to 50% saturation were 1 h 48, 2 h 42, 1 h 30 and 30 min for bulk, P25, anatase and rutile respectively.

3.3. Experiment 2: The effect of nystatin and vanadate on Ti accumulation at 24 h

Nystatin and vanadate incubation increased the level of Ti accumulation for exposures to all the forms of TiO_2 (ANOVA $P < 0.05$), except for rutile TiO_2 when incubated with vanadate (Fig. 3). This net Ti accumulation occurred without changes in cell membrane integrity (e.g., no membrane blebs were observed) and cells remained adhered to the culture dishes throughout. Apical incubations of 100 μmol l^{-1} vanadate caused the largest increases in Ti accumulation relative to the no drug equivalent control (all statistically significant, except for the rutile treatment, $P < 0.05$), resulting in increases above the control value of 10, 12, 12 and 0.9 nmol Ti mg^{-1} cell protein for bulk, P25, anatase and rutile respectively. Similarly, cells incubated with 120 IU ml^{-1} nystatin showed a statistically significant increase in Ti accumulation for all forms of TiO_2 (ANOVA $P < 0.05$) with subsequent increases being 3, 4, 2, and 4 nmol mg^{-1} cell protein for bulk, P25, anatase and rutile respectively above the equivalent no drug control with TiO_2 (Fig. 3).

3.4. Effect of titanium dioxide, nystatin and vanadate exposure on cell electrolytes concentrations at 24 h

There were some TiO_2-dependent changes in electrolyte concentrations in the cells. For example, all forms of TiO_2 (no drugs present) caused some depletion of K^+ and elevation of cell Mg^{2+} concentrations compared to the no added TiO_2 controls (Table 2). There were also some crystal structure effects without drugs, notably an elevation of Ca^{2+} following P25 or the anatase treatments, but not with the other materials (Table 2). These TiO_2-dependent changes in electrolyte concentrations in the cells were all with the electrochemical gradient, but were not associated with non-specific membrane leak (LDH leak remained low).

Incubations of nystatin or vanadate in the absence of TiO_2 caused some changes in cell electrolyte concentrations relative to the drug-free control (Table 2), but there were also some effects of drugs plus TiO_2. For example, in the presence of nystatin, all TiO_2 treatments showed an increase in cell K^+ concentrations. There was a material-type effect with nystatin causing some decrease in cell Ca^{2+} concentrations, but only in the anatase and rutile treatments (Table 2). Cells incubated with vanadate plus TiO_2 exposure showed increases in cell Mg^{2+} for all types of TiO_2. However compared to vanadate alone, the effects on Mg^{2+} were smaller and revealed a material-type effect with the anatase form showing no additional effect relative to the TiO_2 exposure without the drug.

3.5. Experiment 3: The effect of chloropromazine, genistein or amiloride on Ti accumulation at 24 h

Following the primary pharmacological experiments with nystatin and vanadate to broadly determine any involvement of endocytosis or active transport respectively in Ti accumulation, more detailed studies were done with selective inhibitors (Fig. 4). Incubating the cells with genistein in the presence of TiO_2 caused a statistically significant reduction (ANOVA $P < 0.05$) in Ti accumulation relative to the TiO_2 exposure without the drug regardless of material-type (Fig. 4); indicating that genistein may block Ti uptake from all forms of TiO_2. In contrast, incubations with 27 μmol l^{-1} chloropromazine only caused a reduction of Ti accumulation relative to TiO_2 exposure without the drug (ANOVA $P < 0.05$) for the bulk and anatase forms of TiO_2 (Fig. 4). Cell viability with TiO_2 and chloropromazine or genistein was good, with cumulative LDH activity remaining low (0.15 ± 0.5 IU ml^{-1} for both drug trials) and not statistically different from the no drug controls, or the drug controls without TiO_2 (Table 1). There cells showed no membrane blebs and did not detach from the dishes. Overall, suggesting the chloropromazine and genistein effects on TiO_2 accumulation were physiological.

Amiloride had no effect on Ti accumulation from TiO_2 exposures, except for the bulk material which caused a relative increase in the total Ti metal concentration in the cells (Fig. 4). However, the apparent absence of an effect of amiloride on the cells during exposure to the nano forms of TiO_2 may be due to some membrane leak. Amiloride-treated cells exhibited some of the highest cumulative LDH values with or without TiO_2 present (between 0.35 and 0.45 IU ml^{-1} in the external media (Table 1), being significantly higher than the leak in cells without amiloride (ANOVA $P < 0.05$).

Furthermore, visual inspection confirmed the presence of membrane blebbing on the cells. Moreover, the protein content of the amiloride treated cells was lower than expected (<150 mg cell protein well^{-1} compared to values of 400–500 mg cell protein well^{-1} for other treatments) which is likely responsible for the impression of increased or normal Ti accumulation in the cells.

3.6. Effect of chloropromazine, genistein or amiloride on cell electrolytes at 24 h

Although incubations of the cells with drugs in the absence of TiO_2 caused some changes in electrolytes (Table 2, experiment 3), the addition of the different forms of TiO_2 generally had no extra effect on the electrolyte concentrations. However, one notable exception was the effect of genistein on cell Mg^{2+} concentrations which increased in the presence of all forms of TiO_2 compared to TiO_2 exposure without the drug (ANOVA $P > 0.05$, Table 2, experiment 3). The relative increases in Ti accumulation above the control value were 2.2, 5.3, 4.0, 5.5 nmol Ti mg^{-1} protein for bulk, P25, anatase and rutile respectively, but there was no material-type effect on total Mg^{2+} concentrations in the cells.

3.7. Electron microscopy studies to determine TiO_2 particles inside the cells

Electron micrograph images show particles within cells beneath the apical membrane in vesicles or in process of being endocytosed following a 24 h exposure to TiO_2 forms in the absence of drugs (Fig. 5A, C, D and Fig. 6B, C, D). The particles were of the same crystalline morphology as the equivalent electron micrographs from the stock dispersions (Fig. 1), and with the presence of Ti being confirmed by EDS (Figs. 5 and 6). Neither particles nor Ti was present in control cells (Fig. 6A) and there did not appear to be any observable intracellular pathological differences in cells exposed to 1 mg l^{-1} TiO_2 solutions relative to control cells. Fig. 5A, C and D show electron dense material in the scanning electron micrographs, and EDS confirms that these are Ti-rich electron dense areas underneath the apical membrane (i.e., inside the cells) and not between or basolaterally located underneath the cells.

4. Discussion

The present study demonstrates that confluent and electrically tight Caco-2 cells are capable of Ti metal accumulation within a few days of the epithelial forming. The cells will accumulate Ti from TiO_2 particle exposures, and the occurrence of deposits rich in elemental Ti and oxygen underneath the apical (mucosal) membrane suggests at least some of the TiO_2 entered the cells in the particulate form. Caco-2 cells show saturable, drug-sensitive Ti accumulation which is indicative of an active uptake mechanism(s). Critically, the Ti accumulation rate is dependent on the crystal structure of the material, with the nano rutile form being taken up the least. The differential drug sensitivity of the Ti accumulation suggests more than one pathway is involved in Ti accumulation from TiO_2 exposures, and given the ability of Caco-2 cells to actively exclude the rutile form, the possibility of crystal-structure specific pathways cannot be excluded.

4.1. Accumulation of titanium from TiO_2 exposures

The present study showed time-dependent and saturable accumulation of total Ti metal in Caco-2 cells from exposures to TiO_2 particles (Fig. 2). This is indicative of an active accumulation mechanism(s) and cannot be easily explained by passive uptake of dissolved Ti metal down the electrochemical gradient, or by incidental uptake of intact particles through damaged cell membranes. The absence of an appreciable diffusive leak through the apical membrane is confirmed by the low and consistent LDH concentrations in the external media (0.1–0.2 IU ml^{-1}) in the presence of the different forms of TiO_2. The incidental passive uptake of dissolved Ti metal by solvent drag with the major electrolytes is also extremely unlikely, as the cell Na^+ concentrations did not change, and the K^+ gradient is outward, in the opposite direction to that of the net Ti accumulation. In any event, TiO_2 particles are poorly soluble at neutral pH in NaCl-rich gut lumen salines (Al-Jubory and Handy, 2012) or defined NaCl solutions (Schmidt and Vogelsberger, 2009), releasing only picomolar concentrations of Ti metal that would be insufficient to support the accumulation rates observed here from the external medium (Fig. 2).

An active accumulation mechanism is also supported by the effects of addition of inhibitors such as vanadate or nystatin which both increased the net Ti accumulation in the cells (Fig. 3). The rate limiting step in metal uptake by epithelial cells is usually at the basolateral (serosal) membrane where efflux into the blood compartment must occur against the electrochemical gradient; and this is also true for metals like Cu that have a vesicular trafficking system which exudes Cu-containing vesicles at the basolateral membrane by exocytosis (Arrendondo et al., 2000; Handy et al., 2000; Dameron and Harrison, 1998; Kaplan and Lutsenko, 2009; Bury and Handy, 2010). Blockage of the primary ion transporting ATPases on the basolateral membrane, or the ATPases involved in vesicular trafficking to the serosal compartment, will result in the observed net increase in Ti accumulation by the cells (Fig. 3). Similarly, nystatin which sequesters cholesterol to prevent the initiation of the non-specific lipid raft formation needed for membrane invagination during calveolae-based endocytosis (Baro et al., 2001; Nabi and Lee, 2003; Silva et al., 2006) should, at least slow vesicular trafficking through the cell leading to the observed increase of total Ti in the cells (Fig. 3). Al-Jubory and Handy (2012) also showed that nystatin prevented transepithelial uptake of Ti from exposures of TiO_2 particles, and although the form of the Ti was not verified in the cells, this occurred with a concomitant increase of total Ti content of the gut epithelium. Nystatin does not block all modes of endocytosis (clathrin based processes may continue, Chen et al., 2011). Regardless, the observed nystatin-sensitive Ti accumulation (Fig. 3) is indicative of active mechanism(s) for handling either Ti metal or TiO_2 particles by Caco-2 cells.

The total Ti accumulation was between 6 and 14 nmol Ti mg^{-1} cell protein in 24 h for Caco-2 cells for an exposure to 1 mg l^{-1} TiO_2, depending on the form of the material (Fig. 2). This is broadly similar to previous reports on this cell line in DMEM exposed to 1 mg l^{-1} TiO_2 particles (e.g., Koeneman et al., 2010, 160 ng over 24 h). Initial uptake rates which represent the maximum accumulation rate when the experimental system is not at steady-state, appears not to have been previously reported for Caco-2 cells. The initial uptake rates for Ti accumulation were around 3–5 nmol mg^{-1} protein h^{-1} depending on the form of TiO_2 (Fig. 2). This maximum rate of accumulation is broadly similar to that for other metals; notably for copper (trout intestinal cells, 1.8 nmol mg^{-1} protein h^{-1}, Burke and Handy, 2005; Caco-2 cells, 0.1 nmol mg^{-1} protein h^{-1} (the maximum rate of influx using radio labelled copper, Arrendondo et al., 2000)). The initial accumulation rates in the present study are also broadly consistent with the notion of nanomolar rates of uptake in the perfused trout intestine (initial rates of around 1 mg Ti g^{-1} tissue h^{-1} (Al-Jubory and Handy, 2012). This similarity in Ti metal uptake rates with intact intestinal tissue may be fortuitous. While the Caco-2 cell line is a useful model for exploring relative differences between metal treatments, and the mechanisms involved, they are not intended to represent in vivo uptake rates in the human gut. Indeed, it is important to note that Caco-2 cells were originally immortalized from colon cancer cells. Subsequently, carcinoma cells have been shown to have high trace

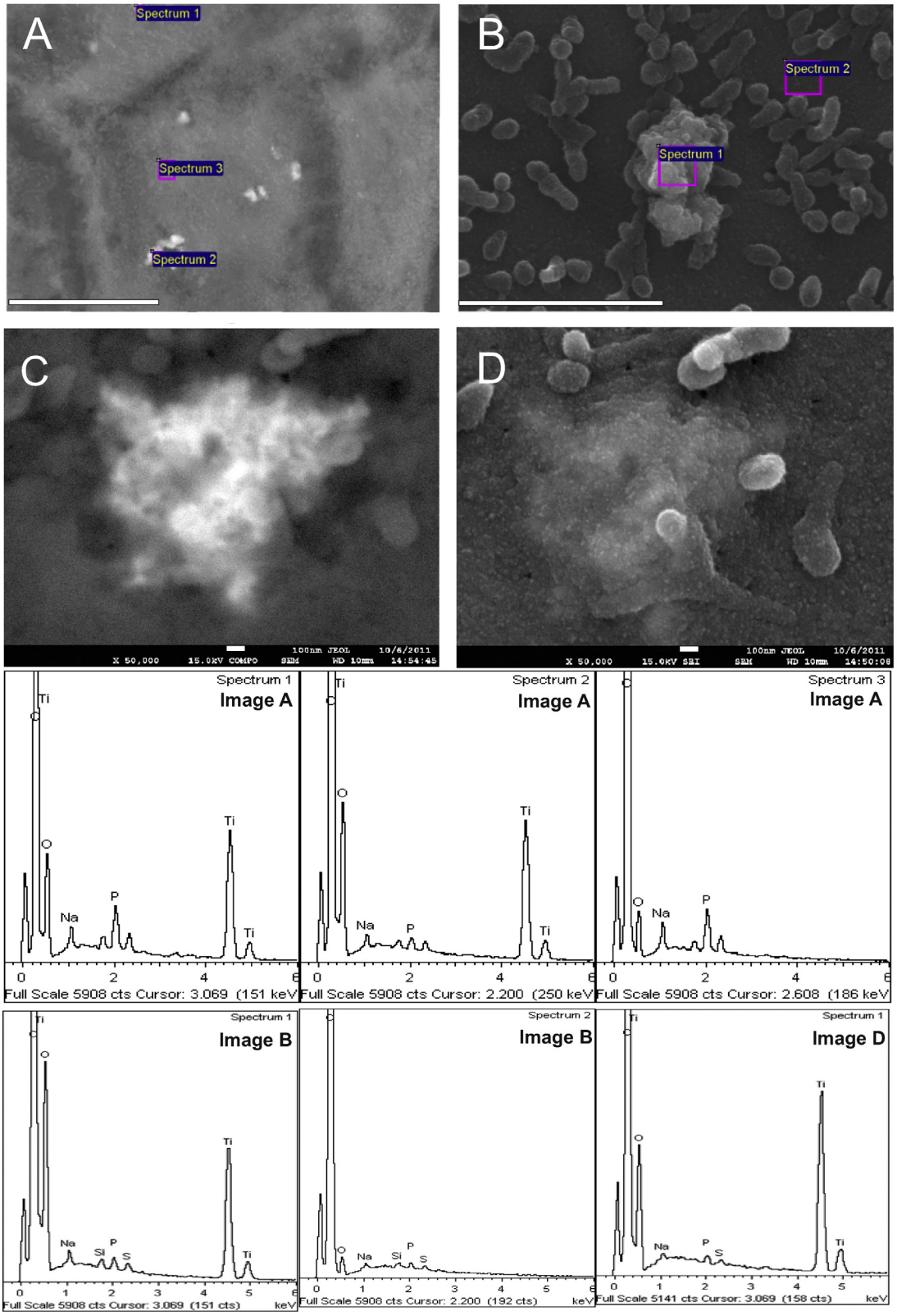

Fig. 5. (A–D) SEM images of Caco-2 cells 96 h after seeding having been exposed to 1 mg l^{-1} TiO_2 forms. (A) Backscatter image (BSI) of Caco-2 cells exposed to 1 mg l^{-1} 'anatase' TiO2'A' showing subsurface Ti with EDS spectra below; (B) Secondary electron image (SEI) of surface bound anatase TiO_2 (scale bar represents 2 μm); (C) BSI of 'D' showing subsurface Ti; (D) SEI image of cell surface exposed to P25 TiO_2. The cell membrane appears to have covered the TiO_2 (projections are microvilli, scale bar represents 100 nm); Spectra are labelled according to which image they belong to. The spectrum labelled Image D is the spectra associated with an EDS map of the entire Image 6 D.

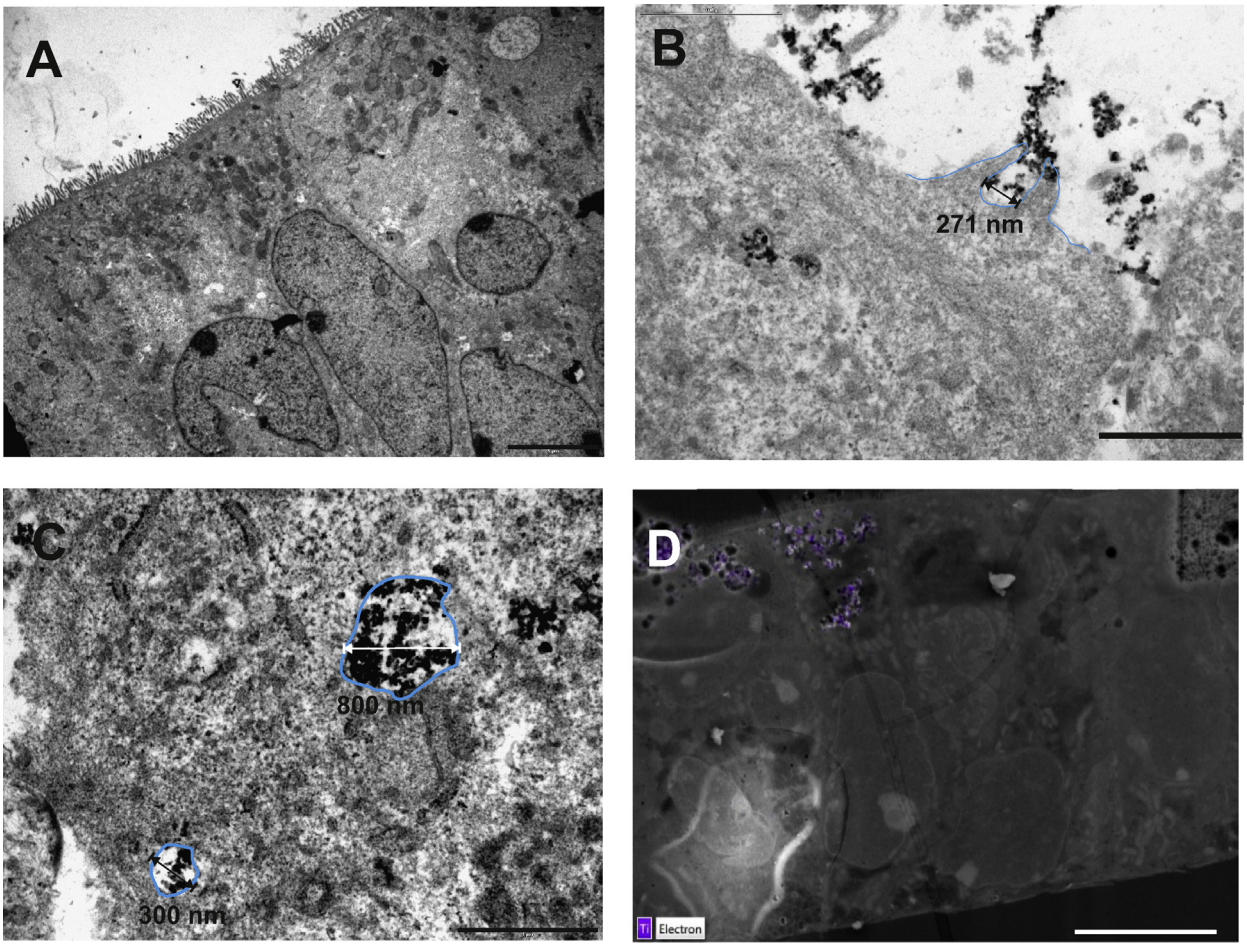

Fig. 6. (A–D) TEM images of cells grown for 21 days in culture inserts; (A) TEM of control cells (scale bar represents 5 μm); (B) TEM image of cells following exposure to 10 mg l^{-1} P25 TiO_2 NPs (Note the invagination in progress (measuring 271 nm across)) (scale bar represents 1 μm; (C) TEM image of intracellular matrix comprising of two vesicles containing NPs (Vesicles are of differing sizes 300 nm and 800 nm diameter, Scale bar represents 1 μm); (D) SEM blockface image in backscatter mode with EDS showing intracellular Ti underneath the apical membrane (scale bar represents 10 μm) The thickness of the monolayer is between 30 and 40 μm.

metal uptake rates due to increased cell proliferation, membrane turnover and higher concentrations of apical membrane metal transporters, which are characteristic of carcinoma cells rather than gut cells (Brookes et al., 2006).

4.2. *Membrane maturity and the absorption of intact TiO_2 particles*

It is well established that Caco-2 cells of only a few days old can be used for metal transport studies, provided the cells are confluent as a polarised monolayer with a steady measurable transepithelial resistance of around 250 Ω cm^2 and/or have demonstrable unidirectional ion fluxes. Indeed, all of these parameters have been shown to occur within 3 days (Peterson and Mooseker, 1993; Yamashita et al., 2002; Zerounian and Linder, 2002; Arrendondo et al., 2006; Moriya and Linder, 2005; Linder et al., 2006; Sonnier et al., 2011). It is perhaps no surprise that electrolyte and trace element transport mechanisms are the first features of intestinal cells to mature (Dharmsathaphorn and Madara, 1990); for without these mechanisms in place, fundamental process to cell survival such as cell volume control would not occur. However, this is the first time that 4-5 day old confluent monolayers of Caco-2 cells have been used to study the accumulation of nano metals. For 'intact' nano particle uptake there may be some concern that the proteins necessary for vacuole formation and vesicular uptake are not yet localised to the apical membrane. This is not the case. Particles can be clearly seen directly under the apical membrane on the inside of the cell (Figs. 5 and 6), with the presence of TiO_2 confirmed by EDS. Moreover, several of the electron micrographs captured the process of vesicular formation and membrane invaginations with particles being captured by the folding membrane (Fig. 6B–D). This strongly suggests active processes, with large folds being reminiscent of macropinocytosis (Fig. 6B–D) and the smaller vesicles likely a form of endocytosis (Fig. 6C). Peterson et al. (1993) also showed F-actin and villin are localised to the apical membrane by day 2–3 in Caco-2 cells. Moreover, Peterson et al. (1993) also showed no statistical differences in the concentration of fodrin and myosin between day 3 and 21 in Caco-2 cells. In short, all the molecular machinery for endocytosis are present in Caco-2 cells very early on after the monolayer is formed and visual evidence of membrane invaginations are present in the current study. Thus Caco-2 cells of 4 days old (post seeding) can be used for both dissolved metal and nanoparticulate metal studies. It was not possible to perform a quantitative analysis of the number of crystals or type within each vesicle from the electron micrographs (Fig. 6), but there appeared to be more aggregates composed of rounded particles rather than striated particles (rutile) in the invaginations and vesicles; tentatively suggesting that the anatase crystal form may be preferentially accumulated by cells. In contrast to research on metals, nutrient absorption studies (e.g., Au and Reddy, 2000) tend to use cells around 21 days old since these express enzymes involved in digestive processes (e.g., alkaline phosphatase activity continues to rise; sucrose-isomaltase localise to the apical membrane). However, the advantage here is that metal transport can be studied without the confounding

factors of nutritional processes, and for example the non-specific digestive vacuoles associated with feeding fully matured cells.

4.3. Effect of particle-size and crystal structure on Ti accumulation

Notably, the type of the TiO_2 influenced the total Ti accumulation over 24 h with the bulk material showing the greatest uptake, and nano rutile TiO_2 the least (Fig. 2). The bulk material effect may simply be explained on a mass basis. For every particle taken up by the cells, the larger bulk TiO_2 would inevitably contain more Ti metal. However, the bulk material stock dispersions did have one of the higher particle number concentrations and mean aggregate sizes (Fig. 1), and it is possible that the bulk material was more bioavailable in the experiments. Al-Jubory and Handy (2012) also noted this behaviour for the same bulk material in gut salines.

There is also some evidence of a true-particle size effect on total Ti accumulation by the cells. In the present study, both the bulk and P25 materials were 25% rutile: 75% anatase. In the time course study, there was generally a lag in uptake of the P25 compared to the bulk material (Fig. 2), and the third series of experiments (Fig. 4) showed a clear statistical difference with less Ti accumulation from the P25 compared to the bulk material. There was also a trend of less Ti accumulation from the P25 compared to bulk material in the second experiment although it was not a statistically significant difference (Fig. 3). Particle-size effects on TiO_2 uptake by Caco-2 cells have been controversial. Unlike, the present study, some reports have used high doses of TiO_2 that caused toxicity (Liu et al., 2006; Trouiller et al., 2009; Koeneman et al., 2010; Ryabchikova et al., 2010)), and are therefore unlikely to be measuring true physiological uptake. Whilst others have used a bulk material of unspecified crystal structure, perhaps not the same as the nano form, making it problematic to separate a true size-effect from any crystal-structure effect in the experimental design (Liu et al., 2006; Wang et al., 2007; Kobayashi et al., 2009; Koeneman et al., 2010).

There was a crystal-structure effect within the nano forms of TiO_2, with the rutile being accumulated less than the anatase or P25 (Fig. 2). This is not readily explained by poor availability of rutile particles in the stock dispersions. Indeed, the rutile form gave the highest particle number concentrations (Fig. 1). Unfortunately, it was not possible to reliably determine the total Ti metal concentrations in the media over the cells for each crystal structure, as particle settling was observed during the experiments especially for the rutile form. Any settling would increase the contact of each test material with the cells. Nonetheless, there may be a biological reason for less Ti accumulation from the rutile TiO_2 NP exposure. One possible explanation is that the Caco-2 cells are using different pathways to take up TiO_2, depending on the form of the material (see below on pharmacology). Alternatively, there may be some aspect of cell surface recognition that excludes one crystal form over another. Interestingly, Ryabchikova et al. (2010) found that brookite and rutile forms of TiO_2 NPs produced different morphologies of membrane invaginations in MDCK cells by electron microscopy. The authors tentatively interpreted these observations as a possible crystal-structure effect on plasma membrane fluidity. However, Ryabchikova et al. (2010) also noted a substantial loss of cell viability that was crystal structure-dependent (up to 60% of the cells staining with trypan blue at 100 $\mu g\,ml^{-1}$ of brookite TiO_2), which could confound their data interpretation as non-physiological.

4.4. Pharmacological investigation and the accumulation of Ti from exposures to different crystal structures

Having demonstrated that Ti accumulation was saturable and sensitive to vanadate or nystatin, more detailed experiments were performed with specific inhibitors (Fig. 4) to determine the pathways involved. These pharmacological investigations were intended to be physiological without causing damage to the cells. This was confirmed by the low LDH activity in the media in the presence of drugs with/without TiO_2 present (Table 1), and the normal morphology of the (adherent) cells in the presence of the drugs. The only exception was a small (0.3 IU ml^{-1}, Table 1), but statistically significant increase in media LDH activity following exposure to 1.25 mmol l^{-1} amiloride. However, this occurred without loss of cell K^+ (Table 2) suggesting the effect was modest.

Chloropromazine is arguably a selective inhibitor of clathrin-mediated endocytosis and the drug prevents the formation of clathrin lattices at the plasma membrane which are essential to initiating the membrane invagination (Wang et al., 2003). In the present study, chloropromazine caused a statistically significant decrease in Ti accumulation in Caco-2 cells for exposure to the bulk (contains anatase) and the nano anatase form, but not the P25 and rutile materials (Fig. 4). This could suggest that the anatase form is somehow better detected for uptake by the clathrin-mediated endocytosis pathway. Such a hypothesis would require a specific receptor-mediated detection of anatase TiO_2 crystals by clathrin-coated pits, but how this might occur is unclear.

Genistein is a tyrosine kinase inhibitor that can be used to manipulate cell volume control via its effects on the actin-cytoskeleton (Akiyama et al., 1987; Wodnicka and Burridge, 1994), and for similar reasons also blocks caveolae-mediated endocytosis pathways (Razani et al., 2002; Van der Ma et al., 2007). In contrast to chloropromazine, genistein decreased the accumulation of Ti from all forms of TiO_2, but had the biggest effects on the rutile and P25 materials (Fig. 4). This might suggest that the rutile form especially is preferentially taken up through caveolae-mediated endocytosis, but the mechanism for this selection is unknown. There is also some cross-talk between the endocytosis pathways in mammalian cells, therefore secondary effects cannot be excluded. For example, genistein may also inhibit F-actin recruitment to clathrin-coated pits and therefore causes a secondary inhibition or delayed uptake via the clathrin-mediated pathway (Zhang and Monteiro-Riviere, 2009). This might explain why genistein also has some effects on the anatase form of TiO_2. A component of clathrin-dependent endocytosis also seems to occur without the involvement of specific receptors (Kirchhausen, 2009).

An alternative hypothesis to crystal structure-specific pathways of endocytosis is incidental size selection into each pathway by particle type. However, this idea is not easily explained by the data. For example, on a size basis, the bulk material might be expected to have its own pathway, but the drug-sensitivity profile (Fig. 4) does not support this. Nonetheless, it is curious that within the nano scale materials, the nano anatase TiO_2 with the smallest primary particle size (16 nm) is the most sensitive to chloropromazine, and the largest nano material (rutile, 30 nm) is effected the most by genistein.

4.5. Ionic regulation in Caco-2 cells during TiO_2 exposure

One of the functions of the gut epithelium *in vivo* is the absorption of nutritionally required electrolytes. Dissolved forms of toxic metals are known to interfere with ion uptake across the gut, and for example, Cu interference with Na^+ homeostasis (Handy et al., 2002). This interference in physiologically functional cells is usually explained by competition for ion uptake down the electrochemical gradient through ion channels, and/or selective inhibition of specific ion transporters. In the present study, direct competition from dissolved Ti^{2+} is unlikely. Although, the Ti^{2+} ion has a crystalline ionic radius smaller than all the electrolytes reported here, except possibly for the Mg^{2+} ion (in order of size: Mg^{2+}, 86 pm; Ti^{2+}, 100 pm; Ca^{2+}, 114 pm, Na^+, 116, K^+, 152 pm, (Shannon, 1976), the

appearance of appreciable dissolved Ti^{2+} in the cell culture medium by dissolution is extremely unlikely (solubility reasons above at neutral pH). In any event, the likely picomolar amounts released would be easily out competed by the millimolar concentrations of the other ions in the media. Nonetheless, TiO_2 exposure caused increases of the total Ca^{2+} concentrations in the cells (Table 2). The reasons for this are unclear, but TiO_2 is reported to interfere with Ca homeostasis in keratinocytes (Simon et al., 2011). There were also some increases in the Mg^{2+} content of the cells during the TiO_2 exposures, and with most of the intracellular Mg^{2+} being normally bound to membranes inside the cell (Romani and Scarpa, 1992; Juttner and Ebel, 1997) this may be incidental Mg^{2+} accumulation with endocytosis of TiO_2 particles. The depolarising effect of the small decrease of the cellular K^+ during TiO_2 exposure (Table 2) would also slow active Mg^{2+} efflux on the Na^+/Mg^{2+} exchanger (see Handy et al., 1996 for the latter).

The combined effects of ion transport inhibitors in the presence of TiO_2 particles on cell electrolyte contents appear not to have been previously reported. In the present study, the combined effect of TiO_2 plus nystatin caused a decrease of cell K^+ concentration compared to the drug alone. The combination of nystatin plus TiO_2 also caused less disturbance to cell Ca^{2+}, with the presence of TiO_2 counteracting the effect of the drug (Table 2). The combined effect of genistein plus TiO_2 also ameliorated the effect of genistein alone to raise Ca^{2+}. The reasons for these interactions require further investigation, and remain unknown.

5. Conclusion

This study shows that Caco-2 cells accumulate Ti from TiO_2 exposures with characteristics that are most easily explained by active uptake of Ti-containing particles in physiologically competent cells. Critically, there is a crystal structure-effect with the anatase form of TiO_2 being absorbed faster than the rutile in time-matched cultures of the Caco-2 cells, indicating this was not a cell maturation effect. From a regulatory perspective, it is therefore not safe to simply extrapolate from one form of TiO_2 to another, and at least some correction factor for the accumulation rates of the different crystal structures should be included in dietary exposure hazard assessments for human health. Moreover, TiO_2 also appears to disturb some aspects of electrolyte status in Caco-2 cells, and like other metals, health effects assessments should consider interference with the nutritionally required minerals.

Author's contributions

C.G. and A.A. conducted the bench work, with both equally conducted the time course assays and pharmacological investigations.C.G. carried out the microscope studies, and drafted the manuscript. R.H. was the principal investigator, directing the experimental design and bench work as well as editing drafts of the manuscript. All authors read and approved the final manuscript.

Conflict of interest

The authors declare that there are no conflicts of interest.

Transparency document

The Transparency document associated with this article can be found in the online version.

Acknowledgments

The authors would like to thank Lynne Cooper, Peter Bond and Glenn Harper for technical assistance. Al-Jubory was financially supported by a scholarship from the Ministry of Higher Education and Scientific Research via the Embassy of the Republic of Iraq. Gitrowski was supported by a strategic scholarship from Plymouth University.

References

Aitken, R.J., Chaudhry, M.Q., Boxall, A.B.A., 2006. Hull Manufacture and use of nanomaterials: current status in the UK and global trends. Occupat. Med.-Oxford 56, 300–306.
Akiyama, T., et al., 1987. Genistein, a specific inhibitor of Tyrosine-specific protein kinases. J. Biol. Chem. 262, 5592–5595.
Al-Jubory, A.R., Handy, R.D., 2012. Uptake of TiO_2 nanoparticles across the isolated perfused intestine of rainbow trout: nystatin, vanadate, and novel gas-sensitive components. Nanotoxicology, 1–20, http://dx.doi.org/10.3109/17435390.2012.735268 (online).
Arrendondo, M., Uauy, R., Gonzalez, M., 2000. Regulation of copper uptake and transport in intestinal monolayers by acute and chronic copper exposure. Biochim. Biophys. Acta 1474, 169–176.
Arrendondo, et al., 2006. Inhibition of iron and copper uptake by iron, copper and zinc. Biol. Res. 39, 95–102.
Au, A.P., Reddy, M.B., 2000. Caco-2 cells can be used ti assess human iron bioavailability from semipurified meal. J. Nutr. 130, 1329–1334.
Baro, A.R., et al., 2001. Lipid rafts required for GLUT4 internalization in adipose cells. PNAS 98, 12050–12055.
Bermudez, E., et al., 2004. Pulmonary responses of mice, rats, and hamsters to subchronic inhalation of ultrafine titanium dioxide particles. Toxicol. Sci. 77, 347–357.
Bockmann, J., Lahl, H., Eckert, T., Unterhalt, B., 2000. Blood titanium levels before and after oral administration titanium dioxide. Pharmazie 55, 140–143.
Bouwmeester, H., et al., 2009. Review of health safety aspects of nanotechnologies in food production. Regul. Toxicol. Pharmacol. 53, 52–62.
Brookes, M.J., et al., 2006. Modulation of iron transport proteins in human colorectal carcinogenesis. Gut 55, 1449–1460.
Burke, J., Handy, R.D., 2005. Sodium-sensitive and -insensitive copper accumulation by isolated intestinal cells of rainbow trout Oncorhynchus mykiss. J. Exp. Biol. 208, 391–407.
Bury, N.R., Handy, R.D., 2010. Copper and iron uptake in teleost fish. In: Handy, R.D., Bury, N. (Eds.), Essential Reviews in Experimental Biology, vol. 2. Society for Experimental Biology Press, London, pp. 107–127.
Cantley, L.C., Marilyn, R.D., Guido, G., 1978. Vanadate inhibits the red cell (Na^+, K^+) ATPase from the cytoplasmic side. Nature 272, 552–554.
Chaudry, Q., et al., 2008. Applications and implications of nanotechnologies for the food sector. Food Addit. Contam. Part A 25, 241–258.
Chen, X., Mao, S.S., 2007. Titanium dioxide nanomaterials: synthesis, properties, modifications, and applications. Chem. Rev. 107, 2891–2959.
Chen, Y., et al., 2011. Cholesterol sequestration by nystatin enhances the uptake and activity of endostatin in endothelium via regulating distinct endocytic pathways. Blood 117, 6392–6403.
Chen, Z., et al., 2006. Acute toxicological effects of copper nanoparticles in vivo. Toxicol. Lett. 163, 109–120.
Dameron, C.T., Harrison, M.D., 1998. Mechanisms for protection against copper toxicity. Am. J. Clin. Nutr. 67, 1091–1097.
Ferin, J., Oberdorster, G., 1985. Biological effects and toxicity assessment of titanium dioxides: anatase and rutile. Am. Ind. Hyg. Assoc. J. 46, 69–72.
Dharmsathaphorn, K., Madara, J., 1990. Established intestinal cell lines as model systems for electrolyte transport studies. Methods Enzymol. 192, 354–389.
Ferin, J., Oberdörster, G., Penney, D.P., 1992. Pulmonary retention of ultrafine and fine particles in rats. Am. J. Respir. Cell. Mol. Biol. 6, 535–542.
Garnett, M.C., Kallinteri, P., 2006. Nanomedicines and nanotoxicology: some physiological principles. Occup. Med. (Lond.) 56, 307–311.
Handy, R.D., Shaw, B.J., 2007. Ecotoxicity of nanomaterials to fish: Challenges for ecotoxicity testing. Integr. Environ. Assess. Manage 3, 458–460.
Handy, R.D., 2003. Chronic effects of copper exposure versus endocrine toxicity: two sides of the same toxicological process. Comp. Biochem. Physiol., Part A: Mol. Integr. Physiol. 135, 25–38.
Handy, R.D., Musonda, M.M., Phillips, C., Falla, S.J., 2000. Mechanisms of gastrointestinal copper absorption in the African walking catfish: copper dose-effects and a novel anion-dependent pathway in the intestine. J. Exp. Biol. 203, 2365–2377.
Handy, R.D., Eddy, F.B., Baines, H., 2002. Sodium-dependent copper uptake across epithelia: a review of rationale with experimental evidence from gill and intestine. Biochim. Biophys. Acta 1566, 104–115.
Handy, R.D., Gow, I.F., Ellis, D., Flatman, P.W., 1996. Na-dependent regulation of intracellular free magnesium concentration in isolated rat ventricular myocytes. J. Mol. Cell Cardiol. 28, 1641–1651.
Iverson, T.G., Skotland, T., Sandvig, K., 2011. Endocytosis and intracellular transport of nanoparticles: Present knowledge and need for future studies. Nano Today 6, 176–185.

Jani, P.U., Mccarthy, D.E., Florence, A.T., 1994. Titanium dioxide (rutile) particle uptake from the rat GI tract and translocation to systemic organs after oral administration. Int. J. Pharm. 105, 157–168.
Juttner, R., Ebel, H., 1997. Characterization of Mg2+ transport in brush border membrane vesicles of rabbit ileum studied with mag-fura-2. Biochim. Biophys. Acta 1370, 51–63.
Kaplan, J.H., Lutsenko, S., 2009. Copper transport in mammalian cells: Special care for metal with special needs. J. Biol. Chem. 284, 25461–25465.
Kirchhausen, T., 2009. Imaging endocytic clathrin structures in living cells. Trends Cell Biol. 19, 596–605.
Kobayashi, N., et al., 2009. Comparative pulmonary toxicity study of nano-TiO(2) particles of different sizes and agglomerations in rats: different short- and long-term post-instillation results. Toxicology 264, 110–118.
Koeneman, B., et al., 2010. Toxicity and cellular responses of intestinal cells exposed to titanium dioxide. Cell Biol. Toxicol. 26, 225–238.
Lewis, S.A., Eaton, D.C., Clausen, C., Diamond, J.M., 1977. Nystatin as a probe for investigating the electrical properties of a tight epithelium. J. Cell Biol. 70, 427–440.
Liu, Q., et al., 2006. Experimental study on toxicity of nanosized titanium dioxide. Modern Prevent. Med. 33, 1211–1212.
Linder, et al., 2006. Vesicular transport of Fe and interaction with other metal ions in polarized Caco-2 Cell monolayers. Biol. Res. 39, 143–156.
Lomer, M.C.E., Thompson, R.P.H., Commisso, J., Keen, C.L., Powell, J.J., 2000. Determination of titanium dioxide in foods using inductively coupled plasma optical emission spectrometry. Roy. Soc. Ch. 125, 2339–2343.
Moriya, M., Linder, M.C., 2005. Vesicular transport and apotransferrin in intestinal iron absorbtion, as shown in the Caco-2 cell model. Am. J. Physiol. 290, 301–309.
Nabi, I.R., Lee, P.U., 2003. Caveolae/raft-dependent endocytosis. J. Cell. Biol. 161, 673–677.
Panessa-Warren, B.J., Warren, J.B., Wong, S.S., Misewich, J.A., 2006. Biological cellular response to carbon nanoparticle toxicity. J. Phys.-Condens. Matter. 18, 2185–2201.
Peterson, M.D., Mooseker, M.S., 1993. An in vitro model for the analysis of intestinal brush border assembly I. Ultrastructural analysis of cell contact induced brush border assembly in Caco-2BBe cells. J. Cell Sci. 105, 445–460.
Peterson, M.D., Bement, W.M., Mooseker, M.S., 1993. An in vitro model for the analysis of intestinal brush border assembly II. Changes in expression and localization of brush border proteins during cell contact induced brush border assembly in Caco-2BBe cells. J. Cell Sci. 105, 461–472.
Plummer, D., 1971. An Introduction to Practical Biochemistry. McGraw-Hill Book Company, UK, pp. 301–309.
Ramsden, C.S., Smith, T.J., Shaw, B.J., Handy, R.D., 2009. Dietary exposure to titanium dioxide nanoparticles in rainbow trout, (Oncorhynchus mykiss): no effect on growth, but subtle biochemical disturbances in the brain. Ecotoxicology 18, 939–951.
Razani, B., Woodman, S.E., Lisanti, M.P., 2002. Caveolae from cell biology to animal physiology. Pharmacol. Rev. 54, 431–467.
Romani, A., Scarpa, A., 1992. Regulation of cell magnesium. Arch. Biochem. Biophys. 298, 1–12.
Ryabchikova, I.E., Mazurkova, A.N., Shikina, V.N., Ismagilov, R.Z., 2010. The crystalline forms of titanium dioxide nanoparticles affect their interactions with individual cells. J. Med. CBR Def. 8, 1–18.
Sayes, C.M., et al., 2006. Correlating nanoscale titania structure with toxicity: A cytotoxicity and inflammatory response study with human dermal fibroblasts and human lung epithelial cells. Toxicol. Sci. 92, 174–185.
Schmidt, J., Vogelsberger, W., 2009. Aqueous long- term solubility of titania nanoparticles and titanium (IV) hydrolysis in a sodium chloride system studied by adsorbative stripping voltammetry. J. Sol. Chem. 38, 1267–1282.
Shannon, R.D., 1976. Revised effective ionic radii and systematic studies of interatomic distances in halides and chalcogenides. Acta Cryst. A32, 751–767.
Shaw, B.J., Handy, R.D., 2011. Physiological effects of nanoparticles on fish: A comparison of nanometals versus metal ions. Environ. Int. 37, 1083–1097.
Silva, L., Coutinho, A., Fedorov, A., Prieto, M., 2006. Competitive binding of cholesterol and ergosterol to the polyene antibiotic Nystatin. A fluorescence study. Biophys. J. 90, 3625–3631.
Simon, M., Barberet, P., Delville, M.H., Moretto, P., Seznec, H., 2011. Titanium dioxide nanoparticles induced intracellular calcium homeostasis modification in primary keratinocytes. Towards an in vitro explanation of titanium dioxide nanoparticles toxicity. Nanotoxicology 5, 125–139.
Singh, S., et al., 2007. Endocytosis, oxidative stress and IL-8 expression in human lung epithelial cells upon treatment with fine and ultrafine TiO_2: Role of the specific surface area and of surface methylation of the particles. Toxicol. Appl. Pharmacol. 222, 131–151.
Sonnier, et al., 2011. TNF-(induced vectorial secretion of IL-8 corresponds to development of transepithelial electrical resistance in Caco-2 cells (2011). Gastroenterology 140, 1044–1045.
Tiede, K., Boxall, A.B.A., Tear, S.P., Lewis, J.D.H., Hassellöv, M., 2008. Detection and characterization of engineered nanoparticles in food and the environment. Food Addit. Contam. Part A 25, 795–821.
Trouiller, B., Reliene, R., Westbrook, A., Solaimani, P., Schiestl, R.H., 2009. Titanium dioxide nanoparticles induce DNA damage and genetic instability in vivo in mice. Cancer Res. 69, 8784–8789.
Van der Ma, et al., 2007. Cellular uptake of cationic polymer- DNA complexes via caveolae plays a pivotal role in gene transfection in COS-7 cells. Pharm. Res. 24, 1590–1598.
Wang, B., et al., 2006. Acute toxicity of nano - and micro-scaled zinc powder in adult healthy mice. Toxicol. Lett. 161, 115–123.
Wang, L.H., Rothberg, K.G., Anderson, R.G., 1993. Mis-assembly of clathrin lattices on endosomes reveals a regulatory switch for coated pit formation. J. Cell. Biol. 123, 1107–1117.
Wang, J., et al., 2007. Acute toxicity and biodistribution of different sized titanium dioxide particles in mice after oral administration. Toxicol. Lett. 168, 176–185.
Wang, J., et al., 2008. Time-dependent translocation and potential impairment on central nervous system by intranasally instilled TiO_2 nanoparticles. Toxicology 254, 82–90.
Wang, J.Y., et al., 2003. Phosphatidylinositol 4 phosphate regulates targeting of clathrin adaptor AP-1 complexes to the golgi. Cell 114, 299–310.
Warheit, D.B., Webb, T.R., Reed, K.L., Frerichs, S., Sayes, C.M., 2007. Pulmonary toxicity study in rats with three forms of ultrafine-TiO_2 particles: Differential responses related to surface properties. Toxicology 230, 90–104.
Weir, A., Westerhoff, P., Fabricius, L., Hristovski, K., Von- Goetz, N., 2012. Titanium dioxide nanoparticles in food and personal care products. Environ. Sci. Technol. 46, 2242–2250.
Wodnicka, M.C., Burridge, K., 1994. Tyrosine phosphorylation is involved in reorganization of the actin cytoskeleton in response to serum or LPA stimulation. J. Cell Sci. 107, 3643–3654.
Yamashita, et al., 2002. New and better protocols for short term Caco-2 cell culture system. J. Pharm. Cell Sci. 91, 669–679.
Zerounian, N.R., Linder, M.C., 2002. Effects of copper and ceruloplasmin on iron transport in the Caco-2 cell intestinal model. J. Nutr. Biochem. 13, 138–148.
Zhang, L.W., Monteiro-Riviere, N.A., 2009. Mechanisms of quantum dot nanoparticle cellular uptake. Toxicol. Sci. 110, 138–155.